INSTITUTE OF PHYSICS PUBLISHING SMART MATERIALS AND STRUCTURES
Smart Mater. Struct. **15** (2006) 295–301 doi:10.1088/0964-1726/15/2/008

Manufacture and characterization of high activity piezoelectric fibres

C R Bowen[1], R Stevens[1], L J Nelson[1], A C Dent[1], G Dolman[2], B Su[2], T W Button[2], M G Cain[3] and M Stewart[3]

[1] Materials Research Centre, Department of Mechanical Engineering, University of Bath, Bath BA2 7AY, UK
[2] IRC in Materials Processing, University of Birmingham, Birmingham B15 2TT, UK
[3] Materials Centre, National Physical Laboratory, Teddington, Middlesex TW11 0LW, UK

Received 13 May 2005
Published 30 January 2006
Online at stacks.iop.org/SMS/15/295

Abstract
Piezoelectric fibres are finding increasing application in a variety of piezoelectric composites, including active fibre composites (AFCs). This paper describes the manufacture and characterization of lead zirconate titanate (PZT) fibres manufactured by viscous plastic processing (VPP). The manufacturing method will be described along with a systematic characterization of the macrostructure, microstructure, phase composition and low and high field piezoelectric properties. A comparison with other available PZT fibres will be made, which demonstrates that the VPP PZT fibres display high piezoelectric coefficients.

1. Introduction

Piezoelectric materials develop an electrical charge when subjected to a force and develop a strain when subjected to an electric field. For these reasons they are commonly used as sensors and actuators. The most common piezoelectric ceramic is lead zirconate titanate, $Pb(Zr, Ti)O_3$ (PZT) and recent research has reported a variety of PZT fibres which have been manufactured by various routes such as sol–gel, extrusion, viscous suspension spinning process, etc; some of which are now commercially available [1–4]. Applications for piezoelectric fibres include 1–3 composites, which are aligned fibres embedded in a polymer matrix for medical transducer and SONAR applications [5, 6]. The advantages of 1–3 composites are low acoustic impedance and high or tailored piezoelectric coefficients, particularly under hydrostatic conditions [5, 6]. In addition, fibre-processing research is driven by interest in the newly developed active fibre composites (AFC), which have a variety of potential benefits over conventional piezoelectric sensing and actuating devices [7, 8].

AFCs were developed in the Active Materials and Structures Laboratory (AMSL) at Massachusetts Institute of Technology (MIT) and patented in 1994 [8]. Since the initial development of AFCs, significant advancement has been made in many areas including fibre manufacture, matrix materials, electrode design, manufacturing techniques and composite modelling [9]. A typical AFC configuration is shown in figure 1 and comprises a monolayer of uniaxially aligned piezoelectric fibres embedded in a polymer matrix between two interdigitated surface electrodes through which the driving voltage and associated electric field is supplied. The aim of the configuration is to combine interdigitated electrodes and a composite architecture in an attempt to overcome some of the limitations associated with monolithic structural actuators. The advantages of the AFC configuration are that the electric field is applied in the direction of actuation and the fibre direction, which results in the larger d_{33} piezoelectric coefficient being utilized (the smaller d_{31} coefficient is often used in other systems). The introduction of fine scale fibres, typically less than 250 μm, into a polymer matrix also means that the composite has a degree of flexibility and is able to conform to the shape of irregular structures [1–4, 10]. It has also been proposed that the combination of interdigitated electrodes and ceramic fibres offers an enhanced toughness and damage tolerance since the fracture of individual fibres does not lead to ultimate failure of the AFC. The unidirectional nature of the fibres creates in-plane actuation anisotropy, allowing torsional actuation and sensing [11]. Multi-ply composites can also be developed which introduce bending or torsion and the applications for AFCs include shape control, structural health monitoring and vibration control [12–14].

The aim of this paper is to describe the manufacture and characterization of PZT fibres manufactured by viscous plastic processing (VPP), a technique originally developed for the fabrication of macro-defect-free cements [15] and

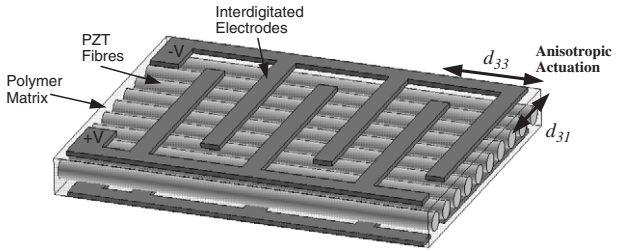

Figure 1. Active fibre composite construction and mode of operation.

subsequently developed for the net shape processing of electroceramic materials [16]. The fibres are intended for incorporation into conventional composite devices (such as 1–3s) or AFCs. The manufacturing route will be initially described, along with detailed characterization of the macrostructure (roundness), microstructure (grain size, density) and phase composition (tetragonal content). In addition, the piezoelectric properties are of importance. Published properties of PZT fibres are often presented at low electric field (<1 kV mm^{-1}) conditions, however during application they are likely to be subjected to high electric field conditions (>1 kV mm^{-1}) where the piezoelectric behaviour can change significantly. For this reason, the high and low field properties of the fibres will be presented. Finally a comparison will be made with other commercially available fibres.

2. Experimental details

2.1. Manufacturing of PZT fibres via VPP

The VPP creates a highly viscous material, composed of ceramic powder particles dispersed in a polymer and solvent gel structure. The material is formed using very high shear forces to break apart any agglomerates in the powder, which are the main cause of defects in brittle materials such as cement and sintered ceramics.

The PZT fibres in this work were manufactured using the VPP technique. Figure 2 shows a schematic diagram of the process. A commercial soft PZT powder (5A, Morgan Electro Ceramics) was mixed with polyvinyl butyral (PVB) binder and cyclohaxane under high shear force using a twin roll mill to produce a viscous plastic dough. Green fibres with diameters of approximately 250 μm were then extruded from a die using the above homogeneous and agglomerate-free dough. After drying, the green fibres were embedded in a Pb-rich zirconia sand bed, and debinding and sintering were carried out at 1 °C min^{-1} to 600 °C for 1 h and 5 °C min^{-1} to 1200 °C for 1 h, respectively.

2.2. Macrostructure and microstructural characterization

The methods utilized in the production of PZT fibre materials will affect both microstructure and morphology, which influences piezoelectric properties and ultimately device performance. To characterize microstructure, two key properties have been investigated: grain structure and porosity. It has been reported that fine-grained materials suffer reduced piezoelectric coupling due to the increased grain boundary interfaces, and that below a critical grain size ($\sim$1 μm) domain formation is impeded [17, 18]. Well-consolidated piezoceramics are required to develop good electromechanical coupling, thus high density and low porosity is desirable for actuator applications and for good mechanical properties [19].

Macrostructural features are also relevant to device manufacture, since active fibre composites require semi-continuous lengths of straight fibres (up to several centimetres in length or more), to achieve an even monolayer with controllable periodicity. Fibre cross section must be consistent along the fibre and between fibres, to avoid defects (such as air-gaps) between the electrode and active material layer that can reduce performance or lead to device failure [20, 21]. Fibre morphology was characterized by image analysis of 100 unique fibre cross sections, to determine shape factors and diameter variability. A sample was prepared with 5 mm fibre lengths, vertically aligned in a potting mould and infiltrated with an epoxy resin. After curing, each sample was ground until planar, polished and gold sputtered before imaging by scanning electron microscopy (SEM) using a Jeol JSM-6310. Digital micrographs were recorded and software enhanced (Paint Shop Pro, Jasc Software) to improve contrast between the fibres and polymer matrix. Image analysis software (ImageTool, UTHSCSA) was used to generate a binary image from which fibres were identified and analysed to compute area (A), and maximum ($D_{\max}$) and minimum ($D_{\min}$) calliper lengths. Results from 100 fibres per material were used to calculate diameter (D_A), elongation (SF_E) and compactness (SF_C) shape factors. Elongation is dependent on the ratio of minimum to maximum calliper diameters

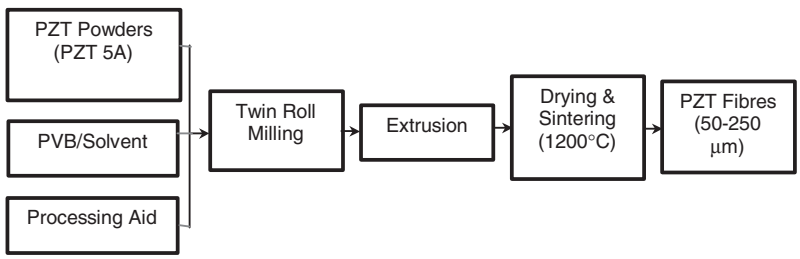

Figure 2. Schematic diagram of manufacturing process for PZT fibres.

(equation (1)), and compactness describes the similarity of a measured feature to a circle (equation (2)).

$$SF_E = \frac{D_{min}}{D_{max}} \quad (1)$$

$$SF_C = \frac{\sqrt{4 \times A/\pi}}{D_{max}}. \quad (2)$$

Both indices have a value of one for a perfect circle and lower values reflect deviation from a uniform cross-section. The best estimation of fibre diameter was found by assuming a circular cross section and calculating the area equivalent diameter, D_A (equation (3)).

$$D_A = \sqrt{4A/\pi}. \quad (3)$$

The sample prepared for morphological study was etched with an HF solution to reveal the grain structure for SEM inspection. To ensure the grains perpendicular to the fibre length were representative of the bulk material, earlier microscopy of exterior grains and fracture surfaces had demonstrated equiaxed grains of comparable dimension. Five randomly selected fibres were examined by SEM and digital micrographs recorded.

Grain size was measured by a linear intercept method due to the efficiency with which large areas can be surveyed. Although the grain size determined by this technique is less than the true grain size, it is a useful comparative parameter. The linear intercept method was followed as described in BS623-3 [22] using image analysis software (ImageTool).

Several common methods exist for determining the density of a ceramic body, which provide approximately equal values for materials of low porosity. Due to practical limitations of handling fine-scale fibres, measurement of apparent bulk density proved the most convenient and reliable approach. One hundred fibres were measured in length (typically 150 ± 0.5 mm), the mass determined on a fine balance (±0.5 mg) and an average density found from the summed measurements and the previously determined average fibre diameter.

2.3. X-ray diffraction

X-ray diffraction was used to (i) identify the phases present and (ii) measure the relative proportion of these phases. Identifying the phases ensured there were no spurious phases other than the desired rhombohedral and tetragonal phases associated with PZT. Measuring the relative proportions of the rhombohedral and tetragonal phases is important to ensure adequate control has been achieved during the production process. Ideally both rhombohedral and tetragonal phases should be present, indicating a composition close to the morphotropic phase boundary (MPB) and enhanced piezoelectric performance. It is difficult to specify an exact composition for optimum activity, but it has been shown that the tetragonal to rhombohedral phase ratio strongly influences d_{33}, d_{31}, and ε_{33}^{T} of fibres [23], as in bulk PZT.

For XRD, sintered fibres in the unpoled state were ground to a fine powder using a pestle and mortar. X-ray diffraction was performed on the powder using a Phillips powder diffractometer fitted with a 4 kW x-ray generator, copper target and a graphite monochromator. Control of the diffractometer was achieved using the supplied diffraction software (PW1877 PC-APD Version 3.5b, Oct. 1999). To assess the phases present a wide-angle scan was performed from two-theta of 20°–60°, while a high-resolution scan was performed in the two-theta range 43°–46° to quantify the phase proportions. Tetragonal and rhombohedral phases are distinguishable on x-ray diffractograms since the {002} planes form a set of reflections in this two-theta range in the form of a doublet and a singlet for the tetragonal and rhombohedral phases respectively [24]. The diffractometer software was used to de-convolute the spectrum into the three distinct peaks associated with the Cu Kα_1 radiation. Integral intensities were calculated for each de-convoluted reflection and the phase content of the rhombohedral phase, P_R, was then calculated from the integral intensities of the Cu Kα_1 reflections using equation (4) [23].

$$P_R = \frac{I_{R(200)}}{I_{R(200)} + I_{T(200)} + I_{T(002)}} \quad (4)$$

where $I_{R(200)}$ is the integral intensity of the (200) reflection of the rhombohedral phase, $I_{T(200)}$ is the integral intensity of the (200) reflection of the tetragonal phase, and $I_{T(002)}$ is the integral intensity of the (002) reflection of the tetragonal phase.

2.4. Piezoelectric properties

The piezoelectric properties of the fibres were characterized by (i) incorporating them into 1–3 composites with a range of fibre volume fractions (v), (ii) characterizing the composites and (iii) calculating the fibre properties from the composite response. Details of this procedure are presented in detail in [25, 26]. The fibres were aligned in cylindrical moulds 2.0 mm in diameter and infiltrated with a low viscosity epoxy resin (Struers Specifix-40) under vacuum to reduce void formation. After curing for 12 h at 40 °C the composites were cut to 5 mm lengths. The composites were polished on their end faces to ensure good electrical contact with the air-dried silver paint, which was subsequently applied. Poling was achieved by applying a field of 2.25 kV mm^{-1} at 100 °C for 10 min. The fibres become poled along their length thus this is designated the 3-direction, while the 1-direction is orthogonal and in the samples radial plane.

2.4.1. Fibre permittivity at low field. The composite permittivity was evaluated from capacitance measurements performed on unpoled composites disks of known geometry and fibre volume fraction at 1 kHz using an HP16451B dielectric test fixture attached to an HP4263B LCR meter using 1 V. The fibre permittivity was calculated from the overall composite permittivity using equation (5).

$$\varepsilon_{33}^{T,composite} = v\varepsilon_{33}^{T,fibre} + (1 - v)\varepsilon_{11} \quad (5)$$

where ε_{33}^{T} is the composite and fibre permittivity at constant stress, v is the fibre volume fraction and ε_{11} is the polymer permittivity.

2.4.2. Fibre d_{33} s_{33}^{E} and k_{33} coefficient at low field. The fibre d_{33} (piezoelectric coefficient), s_{33}^{E} (constant field elastic compliance) and k_{33} (coupling coefficient) were extracted from impedance analysis of composites of known fibre volume fraction over the frequency range 150–500 kHz with an excitation voltage of 500 mV using an Agilent 4194A impedance analyser. Resonance and anti-resonance frequencies were recorded and used to calculate the effective composite properties through the appropriate longitudinal-length mode of resonance. A detailed description of the process is presented in [25]. Fibre properties were extracted from composite properties using an isostrain model and the relationships between composite and fibre d_{33} and s_{33}^{E} are given by the equations (6) and (7).

$$s_{33}^{E,\text{composite}} = \frac{s_{33}^{E,\text{fibre}} s_{11}}{v s_{11} + (1-v) s_{33}^{E,\text{fibre}}} \tag{6}$$

$$d_{33}^{\text{composite}} = d_{33}^{\text{fibre}} \frac{v s_{11}}{v s_{11} - (1-v) s_{33}^{E}} \tag{7}$$

where s_{11} is the elastic compliance of the polymer (357×10^{-12} Pa^{-1} [25]), s_{33}^{E} is the constant field elastic compliance for the fibres in the poling direction, v is the fibre volume fraction and d_{33} is the piezoelectric strain coefficient in the poling direction. The coupling coefficient was calculated using equation (8) [25].

$$k_{33} = d_{33} (\varepsilon_{33}^{T} s_{33}^{T})^{-0.5}. \tag{8}$$

2.4.3. High field strain-field and polarization-field loops. The composite high field strain and hysteresis loops were measured using a system designed and built at the National Physical Laboratory, Teddington, UK. Samples were loaded into the test rig, which was subsequently immersed in oil to prevent electrical breakdown. A sinusoidal voltage was applied to the sample at a frequency of 1 Hz. The current passing through the sample was amplified and used to determine the level of polarization. The sample displacement was monitored using a capacitance sensor, which was mechanically linked to the sample surface via a leaf spring. Butterfly and hysteresis curves were measured at field levels of ± 2 kV mm^{-1}.

The piezoelectric strain of the fibres at electric field E, $S_{\text{piezo}}^{f}(E)$, is related to the composite strain, $\bar{S}(E)$, through equation (8).

$$\bar{S}(E) = S_{\text{piezo}}^{f}(E) \left[\frac{v s_{11}}{v s_{11} + (1-v) s_{33}^{E}} \right]. \tag{9}$$

In which s_{11} and s_{33}^{E} are the compliances of the matrix and fibre respectively (assumed to be independent of electric field). Equation (9) allows the fibre piezoelectric strain-field response to be extracted from measurements of composite strain-field responses, provided the compliance and volume fraction of each phase is known.

The composite polarization at electric field E, $\bar{P}(E)$, can be expressed as a combination of the polarizations developed from three sources, equation (10).

$$\bar{P}(E) = \underbrace{v P^{f}(E)}_{\substack{\text{Fibre contribution} \\ (P_{\text{fibre}})}} + \underbrace{(1-v) P^{m}(E)}_{\substack{\text{Matrix contribution} \\ (P_{\text{matrix}})}} - \underbrace{\frac{v(1-v)(d_{33}(E))^2 E}{v s_{11} + (1-v) s_{33}^{E}}}_{\substack{\text{Clamping contribution} \\ P_{\text{clamp}}}}. \tag{10}$$

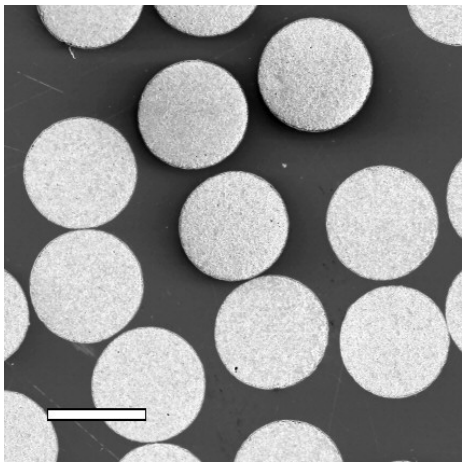

Figure 3. Secondary electron image of VPP fibres in cross section. (200 μm scale bar). Fibres exhibit consistent, circular geometry with little variability between fibres.

In addition to the polarization developed by the fibre, $P^{f}(E)$, and matrix, $P^{m}(E)$, a polarization is developed from active fibre clamping. As an electric field is applied to the composite the fibres strain, but the passive matrix partially clamps the full extension. This clamping effect causes the fibres to develop a charge via their d_{33} effect, which reduces the overall polarization measured. This is quantified as the 'clamping contribution' (P_{clamp}) in equation (10), in which $d_{33}(E)$ is the fibre d_{33} coefficient at electric field E. The importance of this equation is that it enables the polarization response of the fibres to be extracted from the 1–3 composite response, provided the volume fraction and stiffness of each phase, the fibre d_{33} at electric field E, and the matrix permittivity are known since $P^{m}(E)$ is simply the product of the matrix permittivity and electric field.

3. Results

3.1. Macrostructure and microstructural characterization

Values for elongation, compactness and diameter were found to have an approximately normal distribution, hence mean averages were calculated and 95% confidence intervals used to indicate variability. High values for both elongation ($98 \pm 0.2\%$) and compactness ($99 \pm 0.1\%$) reflect a consistent and circular geometry. The shape factors are also well supported by the observed fibre morphology, as illustrated in figure 3. The average diameter was found to be 233 (± 0.8) μm. The associated coefficient of variability was found to be 1.7%, a low value indicating little variation in diameter between fibres of the sample population. Fibre morphology has shown good uniformity, which is highly desirable for the production active fibre composites since this ensures good and consistent contact of the fibres with the interdigitated electrodes [19].

The observed grain structure was randomly distributed, without noticeable orientation or abnormal grain growth (figure 4). From the mean linear intercept values of the fibres studied, an average grain size was calculated that represents in excess of 500 grains. Measurement error in this value was considered to be small, but standard deviation has been

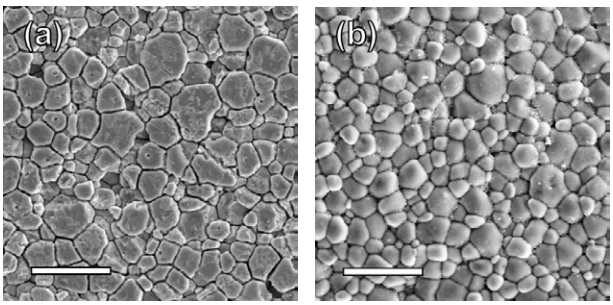

Figure 4. Secondary electron image of grains from (a) polished cross section, (b) exterior fibre surface (10 μm scale bar).

quoted to indicate variability. The grain size of 2.5 ($\pm$0.3) μm is sufficiently large that domain formation is not hindered, and is comparable to values reported for other PZT fibre materials [25].

Calculation of apparent density was limited in accuracy by the uncertainty of the fibre diameter, although due to the large sample population this is not likely to be significant. An estimation of the maximum inaccuracy was possible by considering the propagation of error. The apparent bulk density was found to be 7.7 ($\pm$0.1) Mg m^{-3}. The percentage of the theoretical density of PZT 5A (7.75 Mg m^{-3}) was calculated to indicate a porosity of $\sim$1%, which compares well to microstructural observations. Viscous plastic processing has achieved a dense, well-consolidated material.

3.2. Phase structure

The XRD trace for the fibres is presented in figure 5. The location of the reflection peaks were compared to a reference spectrum for PZT [27]. The reference spectrum was used to assign crystallographic planes to the observed reflection peaks. All reflections can be accounted for confirming the development of the piezoelectric perovskite structure.

The high-resolution scan and its de-convolution into the reflections associated with the tetragonal and rhombohedral phases is shown in figure 5. Using the integral intensities with equation (4), the percentage rhombohedral phase in the fibres is 28%. This confirms the fibres chemical composition is in the MPB region, suggesting compositional control of the fibres has been maintained during processing. Contrary to popular belief, maximum coupling has been shown to occur just outside the two-phase region, on the tetragonal side of the MPB [24]. Therefore a composition with an excess of tetragonal phase is desirable. This suggests the composition of the fibres may not be optimum.

3.3. Piezoelectric properties of VPP fibres

3.3.1. Low field properties and comparison with PZT-5A. Table 1 presents the properties of the VPP fibres determined from the composite measurements. The properties of bulk PZT-5A are also shown for comparison which shows that the properties of the fibres are very similar to those of the bulk material and there has been no significant degradation of properties in forming and sintering the fine scale fibres. This is of importance, since it is possible to experience significant lead loss due the high surface area of the fibres. The results

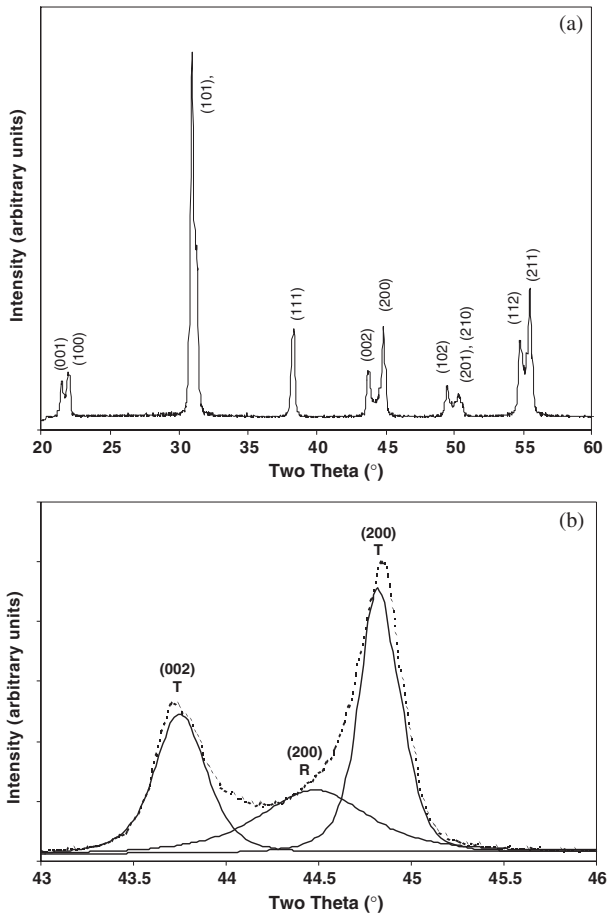

Figure 5. (a) Complete XRD spectrum for the VPP fibres. (b) High-resolution XRD trace (broken line) and its de-convoluted peaks (solid lines) associated with the tetragonal (T) and rhombohedral (R) phases of the VPP fibres.

Table 1. Measured fibre and bulk PZT-5A piezoelectric constants (d_{ij}), relative permittivity ($\varepsilon_{33}^{\mathrm{T}}/\varepsilon_0$), compliance ($s_{33}^{\mathrm{E}}$) and coupling coefficient.

Property (units)	Fibres PZT-5A by VPP	Bulk PZT-5A [28]
d_{33} (pC N^{-1})	377	374
d_{31} (pC N^{-1})	$-$161	$-$171
$\varepsilon_{33}^{\mathrm{T}}/\varepsilon_0$	1650	1700
s_{33}^{E} ($\times 10^{-12}$ Pa^{-1})	18.3	18.8
k_{33}	0.73	0.705

demonstrate that VPP enables high activity powders to be readily formed into fibres without loss of properties.

3.3.2. High field properties. Figure 6 presents typical high-field polarization-field and stain-field loops of piezoelectric fibres, extracted from the response of the composite using equations (9) and (10). The fibre values of saturation strain, saturation polarization and coercive field determined from high volume fraction composites ($v > 0.5$) are summarized in table 2; along with a comparison of properties determined from composites which were manufactured from other commercially available PZT-5A fibres (table 3).

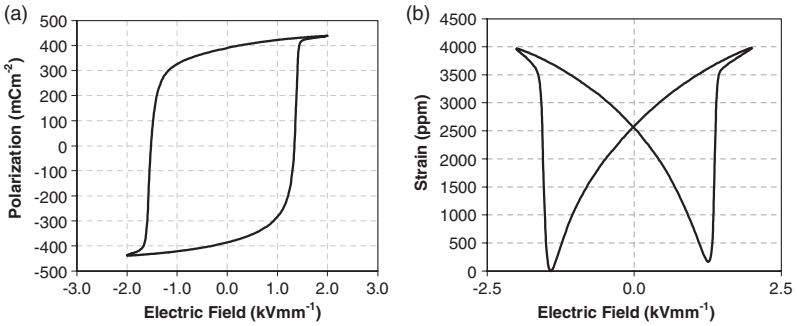

Figure 6. Extracted (a) polarization-field and (b) strain-field loops of VPP fibres.

Table 2. High field parameters of PZT fibres produced by four production methods.

	Saturation strain, S_{sat} (ppm)	Saturation polarization, P_{sat} (mC m^{-2})	Coercive field, E_c (kV mm^{-1})
Extruded	2850	250	1.36
Alceru 250 μm	2950	345	1.10
Alceru 125 μm	3550	425	1.14
VSSP	3950	425	1.04
VPP	4050	400	1.38

Table 3. Details of other PZT-5A fibres for comparison.

Fibre production method	Diameter (μm)	Supplier
Extrusion	130	CeraNova
Alceru	125 & 250	Smart Material Corp.
Viscous suspension spinning process (VSSP)	235	Advanced Cerametrics
Viscous plastic processing (VPP)	233	IRC in Materials, Birmingham, UK

It can be seen from table 2 that the extruded and the Alceru 250 μm fibres develop the lowest strain, both under 3000 ppm. This compares to strains in the region of 4000 ppm for the viscous suspension spinning process (VSSP) and VPP fibres for the same electrical cycle. It is of interest to note that the strain of the smaller diameter Alceru fibres (125 μm) is significantly higher than that developed by the larger diameter fibres. The polarization response of the fibres show that extruded fibres develop the lowest polarization of the fibres tested (250 mC m^{-2}). The 250 μm Alceru fibres develop a slightly higher polarization reaching a saturation polarization in the region of 350 mC m^{-2}. The 125 μm Alceru, VSSP and VPP fibres all exhibit saturation polarizations in the region of 400 mC m^{-2}.

Table 2 also reports the coercive fields for each fibre, a measure of domain mobility. This is invariant with volume fraction, as would be expected. High strain and low hysteretic responses are required for optimum actuator performance. The VPP fibres develop the highest strain, although the polarization response of these fibres exhibits the largest hysteresis (measured from the area of the hysteresis curve). If a lower hysteretic response is required, to minimize heating for example, the VSSP fibres could offer better properties.

4. Conclusions

PZT fibres manufactured using the VPP technique have shown superior piezoelectric properties compared to those from other manufacturing processes. Macrostructure and microstructure characterization has shown that that the VPP fibres have homogeneous structures with good control of size, microstructure and composition. The high piezoelectric coefficient of the VPP fibre indicates that VPP is a promising route for the manufacture of high performance PZT fibres for applications such as active fibre composites.

References

[1] Strock H B, Pascucci M R, Parish M V, Bent A A and Shrout T R 1999 Active PZT fibers, a commercial production process *SPIE Conf. Proc.* **3675** 22–31
[2] Meyer R J, Shrout T R and Yoshikawa S 1998 Lead zirconate titanate fine fibers derived from alkoxide-based sol–gel technology *J. Am. Ceram. Soc.* **81** 861–8
[3] French J D and Cass R B 1998 Developing innovative ceramic fibers *Am. Ceram. Soc. Bull.* **77** 61–5
[4] Meister F, Vorbach D, Niemz F, Schulze T and Taeger E 2003 Functional high-tech-cellulose materials by the ALCER(R) process *Mater.wiss. Werkst.tech.* **34** 262–6
[5] Li K, Chan H L W and Choy C L 2003 Samarium and manganese-doped lead titanate ceramic fiber/epoxy 1-3 composite for high-frequency transducer application *IEEE Trans. Ultrason. Ferroelectr. Freq. Control* **50** 1371–6
[6] Li K, Li J H, Li J C and Chan H L W 2004 Fabrication and properties of PLZT ceramic fiber/epoxy 1-3 composites *J. Inorg. Mater.* **19** 361–6
[7] Bent A A and Hagood N W 1997 Piezoelectric fibre composites with interdigitated electrodes *J. Intell. Mater. Syst. Struct.* **8** 903–19
[8] Hagood N and Bent A A 2000 Composites for structural control *US Patent Specification* 60,48,622

[9] Nelson L J 2002 Smart piezoelectric fibre composites *Mater. Sci. Technol.* **18** 1245–56
[10] Nelson L J and Bowen C R 2002 Determination of the piezoelectric properties of fine scale PZT fibres *Key. Eng. Mater.* **206–213** 1509–12
[11] Bent A A, Hagood N W and Rodgers J P 1995 Anisotropic actuation with piezoelectric fiber composites *J. Intell. Mater. Syst. Struct.* **6** 338–49
[12] Bent A A 1997 Active fibre composites for structural actuation *PhD Thesis* Massachusetts Institute of Technology
[13] Schonecker A, Keitel U, Kreher W, Sporn D, Watzka W and Pannkoke K 1999 Smart structures by integrated piezoelectric thin fibres (II): properties of composites and their physical description *Ferroelectrics* **224** 435–40
[14] Moses R W, Wieseman C D, Bent A A and Pizzochero A E 2001 Evaluation of new actuators in a buffet loads environment *Proc. SPIE* **4332** 10–21
[15] McN Alford N, Birchall J D and Kendall K 1987 High strength ceramics through colloidal control to remove defects *Nature* **330** 51–3
[16] Su B, Pearce D H and Button T W 2001 Routes to set shape electroceramic devices and thick films *J. Eur. Ceram. Soc.* **21** 2005–9
[17] Randall C A, Kim N, Kucera J P, Cao W W and Shrout T R 1998 Intrinsic and extrinsic size effects in fine-grained morphotropic-phase-boundary lead zirconate titanate ceramics *J. Am. Ceram. Soc.* **81** 677–88
[18] Arlt G 1990 Review: Twinning in ferroelectric and ferroelastic ceramics: stress relief *J. Mater. Sci.* **25** 2655–66
[19] Kornmann X and Huber C 2004 Microstructure and mechanical properties of PZT fibres *J. Eur. Ceram. Soc.* **24** 1987–91
[20] Kornmann X, Huber C and Elsener H R 2003 Piezoelectric ceramic fibers for active fiber composites: a comparative study *SPIE Conf. Proc.* **5056** 330–7
[21] Beckert W and Kreher W S 2003 Modelling piezoelectric modules with interdigitated electrode structures *Comput. Mater. Sci.* **26** 36–45
[22] BS EN 623-3:2001: Advanced technical ceramics-monolithic ceramics—general and textural properties—part 3: Determination of grain size and size distribution (characterized by the linear intercept method)
[23] Steinhausen R, Hauke T, Beige H, Watzka W, Lange U, Sporn D, Gebhardt S and Schnoecker A 2001 Properties of fine scale piezoelectric PZT fibers with different Zr content *J. Eur. Ceram. Soc.* **21** 1459–62
[24] Mishra S K, Pandey D and Singh A P 1996 Effect of phase coexistence at morphotropic phase boundary on the properties of $Pb(Zr_xTi_{1-x})O_3$ ceramics *Appl. Phys. Lett.* **69** 1707–9
[25] Nelson L J, Bowen C R, Stevens R, Cain M and Stewart M 2003 Modelling and measurement of piezoelectric fibres and interdigitated electrodes for the optimisation of piezofibre composites *Proc. SPIE* **5053** 556–67
[26] Nelson L J, Bowen C R, Stevens R, Cain M and Stewart M 2003 High field behaviour of piezoelectric fibre composites *Proc. SPIE Smart Struct. Mater.* **5053** 544–55
[27] Powder Diffraction File PDF-2 Database Sets 1-45, International Centre for Diffraction Data (ICDD)
[28] Berlincourt D A, Krueger H H A and Near C 1999 Properties of piezoelectric ceramics *Morgan Electro Ceramics Technical Publication* **226** 1–12